2015

Variability of rock erodibility in bedrock-floored stream channels based on abrasion mill experiments

Eric E. Small

Tevis Blom

Brian M. Hynek

Gregory S. Hancock
College of William and Mary

Recommended Citation

Small, E. E., Blom, T., Hancock, G. S., Hynek, B. M., & Wobus, C. W. (2015). Variability of rock erodibility in bedrock-floored stream channels based on abrasion mill experiments. Journal of Geophysical Research: Earth Surface, 120(8), 1455-1469.

AGU PUBLICATIONS

JGR

Journal of Geophysical Research: Earth Surface

RESEARCH ARTICLE

10.1002/2015JF003506

Key Points:
- A laboratory abrasion mill was used to quantify variations in rock erodibility
- Rock erodibility varies with erosion depth and position in stream channels
- Variations in erodibility are consistent with the expected effects of weathering

Supporting Information:
- Texts S1 and S2, Figures S1–S3, and Tables S1–S3

Correspondence to:
E. E. Small,
eric.small@colorado.edu

Citation:
Small, E. E., T. Blom, G. S. Hancock, B. M. Hynek, and C. W. Wobus (2015), Variability of rock erodibility in bedrock-floored stream channels based on abrasion mill experiments, *J. Geophys. Res. Earth Surf.*, *120*, 1455–1469, doi:10.1002/2015JF003506.

Received 25 FEB 2015
Accepted 7 JUL 2015
Accepted article online 14 JUL 2015
Published online 4 AUG 2015

Variability of rock erodibility in bedrock-floored stream channels based on abrasion mill experiments

Eric E. Small[1], Tevis Blom[1], Gregory S. Hancock[2], Brian M. Hynek[1], and Cameron W. Wobus[3]

[1]Geological Sciences, University of Colorado Boulder, Boulder, Colorado, USA, [2]Department of Geology, College of William and Mary, Williamsburg, Virginia, USA, [3]Stratus Consulting, Boulder, Colorado, USA

Abstract We quantify variations in rock erodibility, K_r, within channel cross sections using laboratory abrasion mill experiments on bedrock surfaces extracted from streams with sandstone bedrock in Utah and basaltic bedrock in the Hawaiian Islands. Samples were taken from the thalweg and channel margins, the latter at a height that is inundated annually. For each sample, a sequence of abrasion mill experiments was completed to quantify variations in erosion rate with erosion depth. Erosion rate data from these experiments shows two things. First, the erosion rate from channel margin samples is greater than for thalweg samples, with the greatest difference observed for the rock surface that was exposed in the stream channel. Second, erosion rate decreases with depth beneath the original rock surface, by an order of magnitude in most cases. The erosion rate becomes steady at depths of 1–3 mm for channel margin samples and 0.1–0.4 mm for thalweg samples. Because only rock properties and microtopography vary throughout the sequence of mill experiments, these results suggest that K_r of the bedrock surface exposed in stream channels is higher at the margins than near the channel center and that K_r decreases over depths of ~1 mm. The simplest explanation for these patterns is that K_r is enhanced, at the bedrock surface and along the channel margins, due to the effects of weathering on rock strength and surface roughness. We hypothesize that a balance exists between weathering-enhanced erodibility and episodic incision to allow channel margins to lower at rates similar to the thalweg.

1. Introduction

Erosion of bedrock-floored channels strongly controls how landscapes respond to climatic and tectonic forcing [e.g., *Whipple,* 2004]. The stream power and shear stress models typically used to describe bedrock erosion [e.g., *Lague,* 2014; *Howard and Kerby,* 1983] are recognized to be broad generalizations of many complex and interacting processes and environmental constraints. The stream power models include four basic factors: slope, drainage area, a measure of sediment availability or cover, and resistance to erosion or erodibility. Climate and hydrology partly control the erodibility, as they dictate the frequency and magnitude of erosive flows [*Tucker,* 2004]. The resistance to erosion is also controlled by the characteristics of the bedrock exposed in the streambed, here referred to as rock erodibility. This rock erodibility influences erosion in several different ways. Rock erodibility is related to intrinsic rock properties such as tensile strength, which have been demonstrated to control erosion due to abrasion [*Sklar and Dietrich,* 2001]. The presence and distribution of rock discontinuities, such as fractures and joints, determines the relative efficiencies of plucking and abrasion [*Whipple et al.*, 2000a, 2000b]. The roughness of the rock surface, which is partly controlled by rock properties and partly by patterns of erosion, also impacts erosion rate [e.g., *Hancock et al.*, 1998; *Huda and Small,* 2014]. In many cases, spatial variations in rock erodibility are found to exert a primary control on the longitudinal profile of bedrock streams [e.g., *Han et al.,* 2014; *Duvall et al.*, 2004; *Allen et al.*, 2013]. Cross-channel variations in rock erodibility may be equally important as a control on channel geometry, channel slope, and the cross-channel pattern of erosion rates [*Hancock et al.,* 2011].

Here we quantify variations in rock erodibility within channel cross sections using laboratory abrasion mill experiments on bedrock surfaces extracted from streams. Rock erodibility is a primary factor controlling erosion rates in channels and is incorporated into models to predict bedrock erosion rates. *Whipple* [2004] provides a model that explicitly includes rock erodibility,

$$E = K_r K_c K_{\tau cr} \ f(q_s) A^m S^n$$

where E is rock erosion rate; K_r represents controls on erodibility (lithology, hydraulic roughness, and channel width); K_c represents climatic conditions; $K_{\tau cr}$ represents the threshold shear stress for incision; $f(q_s)$ represents

sediment load; A and S represent drainage area and channel gradient, respectively; and m and n are theoretically or empirically derived.

Throughout this paper, the term rock erodibility, K_r, refers to a characteristic of the rock that linearly scales the erosion rate in stream power models, holding all other factors constant [e.g., *Hancock et al.,* 2011, equation 4]. In the erosion mill, the flow characteristics (i.e., "channel width") are effectively constant, although small changes in the flow field may result from changes in sample microtopography. Therefore, K_r as used here is composed of only two factors: (1) rock properties, which control the erosion rate given some transfer of energy to the bed via sediment impacts and (2) hydraulic roughness associated with microtopography at the scale of the mill sample (millimeters to centimeters). As we have narrowed the variables to rock properties only, the erosion rates measured in the abrasion mill are directly indicative of the relative magnitude of K_r. When the mill erosion rate is high, it indicates that K_r is high, and vice versa.

Physical and chemical weathering processes should increase K_r, relative to the value for the same rock in an unweathered state. Therefore, weathering is recognized as a potentially important process in the evolution of bedrock-floored channels [*Wohl et al.,* 1993; *Howard*, 1994, 1998; *Whipple et al.*, 2000a; *Turowski et al.,* 2009; *Hancock et al.,* 2011; *Han et al.,* 2014]. Weathering reduces rock tensile strength [*Aydin and Basu*, 2006], and laboratory experiments have documented a relationship between rock tensile strength and resistance to abrasion by bed load saltation [*Sklar and Dietrich,* 2001]. Hence, weathering may also increase the erodibility of rock by abrasion and may also accelerate block plucking by expanding fractures along which blocks are removed [*Hancock et al.,* 1998; *Whipple et al.,* 2000b]. Field observations [*Montgomery,* 2004; *Stock et al.,* 2005] and numerical experiments [*Hancock et al.,* 2011; *Han et al.,* 2014] suggest that weathering can influence channel form and gradient, which in turn partly control erosion rates.

In previous studies, three different types of spatial variability in K_r caused by weathering have been discussed. Each pattern reflects interactions between reductions in K_r due to weathering and the resulting increase in erosion rates. First, K_r may vary throughout a drainage basin, due to spatial patterns of precipitation or temperature and their influence on weathering rate [e.g., *Han et al.,* 2014; *Craddock et al.,* 2007]. Second, K_r may vary across channel cross sections. The efficiency of different weathering processes should vary across stream channels, particularly for processes that are accelerated by periodic rock inundation and proximity to water. *Montgomery* [2004] and *Stock et al.* [2005] describe an extreme example in channels floored by sandstone and siltstone susceptible to weathering via mineral hydration. Other weathering processes should also vary in intensity across channels, including frost action [e.g., *Matsuoka,* 1990], oxidation of Fe^{2+}-bearing minerals, and biologically enhanced weathering [e.g., *Phillips et al.,* 2008]. This is important because cross-channel variations in erosion rate depend on how localized flow conditions, sediment transport and deposition, bed morphology, and rock erodibility interact [*Sklar and Dietrich,* 2004; *Montgomery,* 2004; *Turowski et al.*, 2008a, 2008b; *Hartshorn et al.*, 2002]. *Hancock et al.* [2011] hypothesized that interactions between weathering and erosion may yield higher K_r along channel margins, where stripping of rock by erosion is less frequent, which is balanced by lower shear stress and erosivity in these locations.

The third spatial pattern caused by weathering is that K_r of the exposed bedrock surface may be greater than K_r of the underlying rock. Many weathering processes act more quickly at the interface between rock and water or air than beneath the rock surface, leading to the ubiquitous presence of weathering rinds [e.g., *Sak et al.,* 2004]. The presence of soil or sediment cover may accelerate weathering [e.g., *Heimsath et al.,* 1997], but the affects are still greatest at the bedrock surface that is in contact with the overlying material. *Howard* [1998] and *Hancock et al.* [2011] proposed models for how weathering would change erodibility with depth beneath the rock surface exposed in streams. In both models, a range of outcomes exists due to the interactions between the timescale and depth of weathering and the frequency and magnitude of erosional events. The existence of vertical variations in K_r, caused by weathering or other factors, has not been documented in a quantitative fashion.

Here we quantify variability of rock erodibility in streams, using the abrasion mill method of *Sklar and Dietrich* [2001]. Therefore, the results presented below are relevant to locations where abrasion by bed load dominates. Unlike previous studies, we present abrasion mill measurements from actual rock surfaces exposed in stream channels, as opposed to saw-cut surfaces (L. Sklar, personal communication, 2010) or polyurethane foam [*Scheingross et al.,* 2014]. Field measurements of erosion rate [e.g., *Hartshorn et al.,* 2002]

Table 1. Field Site Characteristics[a]

Stream and Location	Drainage Area (km^2)	Channel Slope	Width/Depth at Upper Location (m)	Calculated Discharge at Upper (m^3/s)
		Sandstone Bedrock		
Onion Creek, Utah	47	0.02	5.4/0.5	1.3
		Basaltic Bedrock		
West Wailua Iki, Maui	10.5	0.06	18/1.9	24 (42)
East Wailua Iki, Maui	9.8	0.065	23/2.5	53
Nanue, Hawaii	15.8	0.045	15/2.2	22

[a]Discharge is calculated using Manning's equation with $n = 0.035$ at Onion Creek and $n = 0.05$ at Hawaiian stream sites. Onion Creek calculation is based on a rectangular cross section, Hawaiian stream calculations based on a triangular cross section. Value in parentheses is based on rating curve at upstream gauge of West Wailua Iki Stream.

do not provide the same type of information about spatial patterns of rock erodibility because it is not possible to isolate the effects of K_r from other factors that also vary across channel cross sections (e.g., flow characteristics and sediment distribution). The focus of this effort is on quantifying variations in K_r, not establishing causal links between weathering and erodibility. However, we do provide supporting information to gauge the degree of weathering in the samples analyzed. This allows us to assess if the observed variations of K_r are consistent with expectations described in prior research.

We use the abrasion mill data to quantify (1) if K_r varies with depth beneath the rock surface and (2) if K_r differs between the channel thalweg and margins. These are two of the patterns in K_r that are hypothesized to exist in bedrock streams as a result of interactions between weathering and erosion. We do not focus on differences in K_r between rock types or variations within a rock type at the scale of drainage basins. The plan of this paper is as follows. Section 2 first describes the sampling procedure, the bedrock samples, and the laboratory and field measurements. This section also describes how the abrasion mill data were analyzed. Section 3 describes the abrasion mill results and the data analyses. In section 4, we discuss how the measured patterns of K_r are consistent or inconsistent with the expected effects of weathering.

2. Methods

2.1. Collection of Stream Bedrock Samples

Samples were taken from streams with sandstone bedrock in Utah and basaltic bedrock in the Hawaiian Islands (Table 1). The streams were selected based on the following criteria. First, all streams had extensive bedrock exposure and intact bedrock across the entire channel. Second, there were no bridges or dams upstream of the sample site. Third, the stream profile, bedrock exposure, and sediment distribution at the sampling site were not affected by roads alongside the channel. Fourth, roads downstream of the site were close enough to allow for the transport of equipment used to extract intact bedrock samples. At the Utah sandstone sites, 20.3 cm diameter bedrock disks were extracted from the bedrock in the channels using a core drill powered by a portable generator (Figure 1). Core samples were drilled perpendicular to the surface, so even if the bedrock surface was sloping, the surface of the sample is generally horizontal in the abrasion mill. Due to steep valley walls in Hawaii, large rocks were quarried from the streambed and mill samples were drilled out of the quarried rocks after they were hauled out from the streambeds, again perpendicular to the original surface.

Our initial goal was to sample bedrock from gauged streams, to provide information regarding the magnitude and frequency of flows at the study sites. However, the third and fourth criteria above required that we eliminate nearly all of the streams visited during reconnaissance, including most gauged streams. As a result, streamflow records are only available for one of the sample locations. For the other steams, we are limited to rough estimates of flow based on channel geometry and Manning's equation. As described below, samples locations were selected based on geomorphic indicators of high flow and dominant erosion process, so knowledge of the flow depth and discharge record at the site is not essential.

A total of 12 samples were collected and analyzed, 6 from streams with sandstone bedrock and 6 from streams with basaltic bedrock. At all sites, bedrock samples were collected from two locations: (1) the lowest point in the channel cross section, referred to as the thalweg sample and (2) a sample closer to the active

Figure 1. Photograph of field sites. (left) Onion Creek, Utah. (right) Nanue Stream, Hawaii.

channel margin, referred to as the upper sample. All thalweg samples were submerged by <10 cm of water during sampling, interpreted to be base flow. The elevation of the upper sample (relative to the thalweg) was selected to ensure that the location was inundated roughly annually: below short-lived high water marks (e.g., grass stranded on branches) and areas with persistent vegetation and soil development, and significantly above the low water level that existed when the samples were extracted. Both thalweg and upper samples were taken from areas of bedrock that exhibited features indicative of abrasion (e.g., potholes or flutes). This does not preclude the possibility that plucking may have occurred in these locations, which would affect the degree of weathering of the sample surface.

Sandstone samples were taken from Onion Creek in eastern Utah (Table 1 and Figure 1). The drainage area of Onion Creek above the sampling site is 47 km^2. Onion Creek is perennial, although base flow is $< 0.2\ m^3\ s^{-1}$. Using Manning's equation and topographic survey data, we estimate that a discharge of $1.3\ m^3\ s^{-1}$ inundates the upper samples collected between 0.3 m and 0.5 m above the channel thalweg. There is extensive sandstone exposed in the channel for ~1 km along the study reach. The bedrock is arkosic sandstones of the Permian Cutler Formation. Within this unit, there is significant stratigraphic variability in rock characteristics, including bedding thickness and secondary mineralogy. The two samples that make up each thalweg-upper pair were extracted from the same bed traced along strike from the channel center to the channel margin. Exact sample locations were chosen at random, although many possible drill sites were excluded due to constraints of securing the drill rig in a wet stream channel.

The characteristics of the exposed sandstone at Onion Creek varied within the sampled reach. Within and adjacent to the thalweg, the rock tends to be fluted, polished, and smooth, and lack significant evidence of plucking (e.g., plucked blocks and voids in the channel left by block removal) (Figure 1). In the upper portions of the cross section ($>$1.5 m above the thalweg), the thin, subhorizontal beds of the sandstone create variable relief on the steep slopes of the valley wall. Hence, plucking may be important on the channel margin and valley wall during the highest flows.

Basaltic rocks were collected from three perennial streams in the Hawaiian Islands. The Hawaiian streams differ dramatically from Onion Creek: annual precipitation is approximately 5 times higher, channel slopes are steeper, and discharge is more than an order of magnitude greater (Table 1). In the gauged basin, annual maximum discharge varies from 30 to 280 m^3/s, corresponding to flow depths of 1.5 to $>$4 m at the gauging site. Upper samples were located approximately 2 m above the thalweg samples. Large waterfalls and steps exist along the profiles of streams we studied. However, the reaches from which we sampled bedrock had smooth profiles with slopes varying between 3 and 8%.

The characteristics of the exposed basalt varied within each study reach. Some areas of exposed bedrock exhibited smoothed surfaces, potholes, and fluting, indicating abrasion occurs [*Whipple et al.,* 2000b]. Nearby, joints were well developed and bounded large intact blocks exposed along the streambed.

Potholes and fluting are absent from these blocks, suggesting plucking is the dominant erosion process. Features indicative of abrasion dominate the center of the channel. In contrast, the channel margins show a mixture of areas indicating abrasion and plucking, with the extent of plucking features increasing with height above the thalweg. In addition, some stratigraphic units are dominated by joint blocks, both in the middle and at the edge of channels. These stratigraphic units tend to produce steps in the otherwise smooth profile and were not sampled in this study.

2.2. Abrasion Mill Experiments

We tested the hypotheses presented above by completing a sequence of abrasion mill experiments, using the mill design of *Sklar and Dietrich* [2001]. The abrasion mill is appropriate to quantify variations in K_r because flow conditions and sediment load can be held constant. Water circulates rotationally around the 20.3 cm (8 inch) diameter mill driven by a propeller 25 cm above the rock surface. In all experiments, we measured the erosion rate from the actual bedrock surface exposed in the stream channel, rather than flat, saw-cut surfaces, as in *Sklar and Dietrich* [2001]. All other aspects of the experimental design follow *Sklar and Dietrich* [2001]. The mass removal rate in the mill was calculated based on the change in mass and the duration of each mill run. The term "mill run" refers to a single-abrasion mill experiment in which a preweighed sample is placed in the mill, is subjected to saltating grains for a set time interval, and then reweighed. We consider the mass removal rate to be linearly related to K_r.

Mass removal was converted to average erosion depth using (1) measured rock density (2.35 g cm^{-3} for sandstone and 2.80 g cm^{-3} for basalt) and (2) the portion of sample surface area over which most of the erosion occurred. We then compared average erosion rate as a function of erosion depth for each sample. Repeat measurements of sample microtopography showed that approximately 80% of the erosion occurs over 50% of the sample area (Text S1 and Figures S1 and S2 in the supporting information). This is due to a secondary circulation within the mill, upward in the middle of the mill, and downward along the edges, consistent with *Sklar and Dietrich* [2001]. We used a single value for "eroded area" (50%) to scale the mass removal measurements to erosion depth. While the mill erosion rates do not scale directly to erosion rates in real streams, variations in erosion rate with depth are related to actual changes in rock properties over the thickness of material removed. Therefore, it is important to make adjustments for the actual eroded area. It is unlikely that the actual eroded area was 50% for all samples during all mill runs. If the actual eroded area is larger (e.g., 60%), then the reported erosion depth is an overestimate. However, observations show that the spatial pattern of erosion was relatively constant (Figure S1 and S2). Thus, the scaling from mass to erosion depth introduces only limited uncertainty when compared to the order of magnitude variations in erosion rate measured in our mill runs. This issue is addressed further in the discussion.

All mill runs were completed using 150 g of sieved 4–8 mm gravel, the mass and grain size that yielded maximum erosion in *Sklar and Dietrich* [2001]. In the experiments of *Scheingross et al.* [2014], sediment of this size was transported exclusively as bed load, consistent with observations made during our mill experiments. Gravel used in the experiment was ~85% quartzite, collected from a tributary to Clear Creek, Colorado. The gravel used for all the experiments was first mixed in a large bin. New gravel was used for each mill run, to avoid changes in the roundness and grain size of the abrading sediment resulting from the mill action.

Preliminary mill experiments showed that the erosion rate from some samples decreased by more than an order of magnitude as the top several millimeters of rock was removed. This presented a challenge in developing an experimental design: the sequence of mill runs used for each sample, hereafter referred to as the "mill sequence," needed to satisfy two opposing criteria. The individual mill runs had to be short enough so that changes in erosion rate were not obscured by long measurement intervals. At the same time, the duration of individual mill runs needed to be long enough to allow for measureable mass loss even when the erosion rate was low. We chose a constant duration for a majority of the mill runs, 2 h for sandstone and 4 h for basalt (Table S1). These durations are short enough to quantify variations in erosion rate that occur over erosion depths < 1 mm, but still long enough to yield measurable erosion after ~100 h of mill abrasion when the mass loss rate has greatly decreased. We interspersed longer duration mill runs between sets of equal length mill runs, yielding measurements of abrasion that spanned a greater depth range of erosion (Figure 2). Total mill time was 90 h over 28 mill runs for each sandstone sample and 174 h over 24 mill runs for each basalt sample (Table S1). All mill data are available in Table S2 (sandstone) and S3 (basalt).

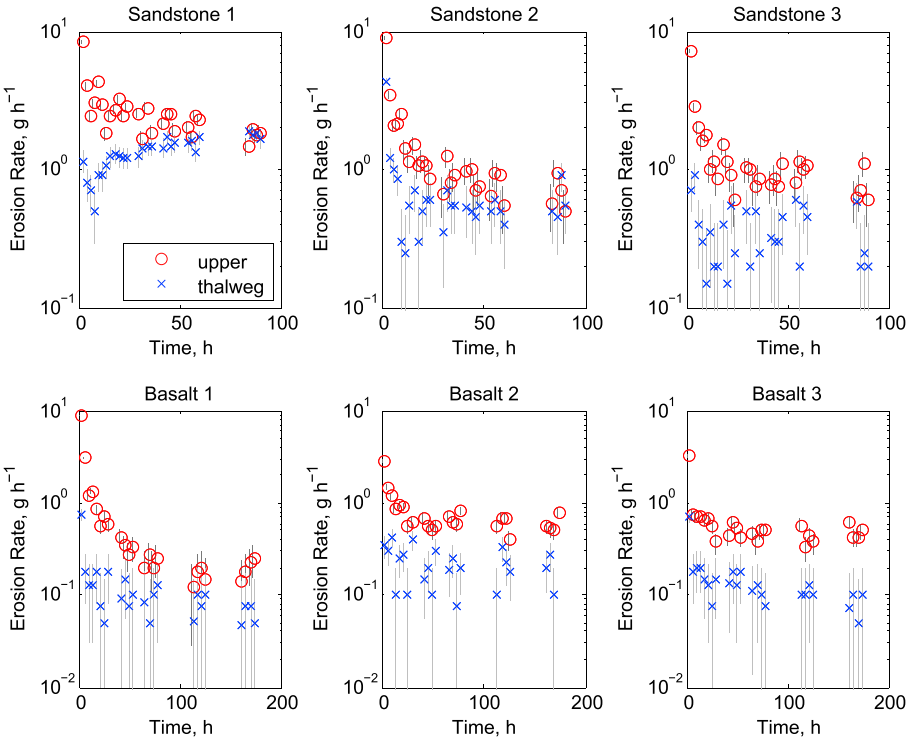

Figure 2. Plots of erosion rate versus time through the mill sequence for upper samples (circle) and thalweg samples (cross). Each point represents the time-averaged erosion rate for an individual mill run. The points are plotted at the cumulative time in the mill sequence at which the mill run ended (see Table S1 for details of mill run times and Tables S2 and S3 for data). Error bars represent the standard deviation (arithmetic) of the blank runs, which differ for basalt and sandstone samples. Error bars from corresponding upper and thalweg samples are offset slightly (in time) for clarity.

Before starting the mill sequence, samples were submerged in water for approximately 1 week until they were saturated. Samples remained saturated throughout the experiments and were removed from the mill for measurements of mass loss. The porosity of all samples was less than 10%. Therefore, we assumed that the measured mass loss due to water trapped in pores was negligible. The surface of the sample was towel dried prior to weighing. Sample mass varied from 2–4 kg and the balance used for measurements had a precision of 0.1 g.

We quantified the repeatability of the abrasion mill experimental procedure to gauge the uncertainty of the data from the mill experiments. We replicated the abrasion mill procedure, including placing the sample in the mill and filling the mill with water and sediment, but without activating the propeller. These blank runs were of similar duration to the standard runs. For sandstone, the rate of change of mass during blank runs was -0.02 ± 0.21 g/h ($n = 8$). In comparison, the average erosion rate during the individual mill runs with sediment was 1.9 g/h. The rate of change in sample mass during basalt blank runs was 0.01 ± 0.09 g/h ($n = 6$), compared to 0.65 g/h for the actual mill experiments. This demonstrates that the mill procedure (without flowing water and moving sediment) does not yield appreciable gain or loss of sample mass. We use the standard deviation of the blank run erosion rate as a measure of experimental error, shown as error bars in Figures 2 and 3. The experimental error from blank runs differs from the error bars shown by *Scheingross et al.* [2014]. Their error bars show variability in erosion rate across actual experiments, including both contributions from both experimental repeatability and variations in sediment and substrate characteristics.

2.3. Quantifying Changes in Erosion Rate and Erodibility With Depth

We examine three aspects of the erosion rate data: (1) Does the erosion rate decrease with depth beneath the bedrock surface that was originally exposed in the streambed, implying lower K_r with depth? (2) Does the erosion rate reach a nearly constant value at some depth, which we refer to as the Steady State Erosion Depth (SSED)?; and (3) what is the erosion rate once the SSED is reached, which we refer to as the Steady State Erosion Rate (SSER).

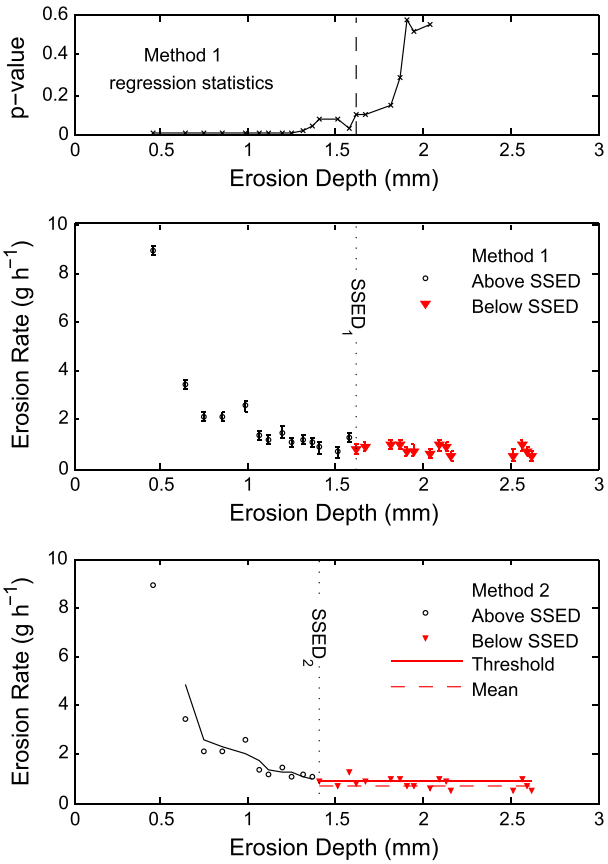

Figure 3. (top) Regression statistics used in method 1 to identify evidence of a nonzero slope, from the Sandstone Upper 2 data. Each point is the *p* value for a linear regression that includes all data from that erosion depth and below. Dashed line indicates the SSED determined via method 1. (middle) Erosion rate versus erosion depth for Sandstone Upper 2. The steady state erosion depth from method 1 ($SSED_1$) is marked by the vertical dashed line (1.62 mm). Error bars represent the standard deviation of the sandstone blank runs. (bottom) Same data analyzed with method 2. $SSED_2$ is marked by the vertical dashed line. The three-sample average erosion rate is shown by the black descending line. The red solid line shows the threshold (mean + 1 standard deviation), below which the three-sample average must fall for the SSED to be reached. The red dashed line shows the mean for the last seven mill runs ($SSER_2$).

Using the mill data to address these questions is not straightforward. There is no accepted model for how K_r varies with depth beneath the exposed bedrock surfaces to guide this analysis. *Hancock et al.* [2011] used a numerical model to simulate vertical variations of K_r in stream bedrock, incorporating a weathering function that decreased exponentially with depth. However, the resulting vertical K_r profile was not necessarily exponential, due to interactions between weathering and erosion. We have found no analogy in the geomorphology literature to guide this data analysis. Methods exist to identify a breakpoint that separates a times series into two (or more) parts with different trends [e.g., *Solow,* 1987]. We describe our implementation of this type of approach below (method 1). We also developed a second simpler method to provide results for comparison to the first method.

2.3.1. Method 1: Identify a Breakpoint

For each sample, the erosion rate data from the mill sequence are used to evaluate if a breakpoint exists that separates the vertical profile of erosion rates into two segments: (1) a lower section in which the erosion rate does not vary with depth and (2) an upper section in which it does. The breakpoint corresponds to the $SSED_1$, the subscript denoting the value corresponds to the first method. Method 1 allows for the possibility that erosion rate does not vary throughout the entire depth profile. In this case, $SSED_1$ is at the rock surface. This method also allows for the possibility that the erosion rate varies throughout the profile, although this was not the case for any of the samples.

The following procedure is completed separately for each sample using the data measured during that sample's mill sequence. Because the mill data shows steady values at the end of the sequence, and not at the beginning, our assessment of the presence of a linear slope begins at the end of the mill sequence, and then proceeds forward toward the beginning. We start by using the erosion rate and cumulative erosion depth data from only the last 7 mill runs (e.g., runs 22–28 for sandstone, Table S1). For all 12 of the samples, the slope is not different from zero using this subset of data—there is no evidence that abrasion varies with depth. The regression is then repeated including the data point from the preceding mill run (e.g., runs 21–28 for sandstone) and the likelihood of a nonzero slope is evaluated (Figure 3, top). The process is repeated, sequentially including data from preceding mill runs, until all the data are included. Regression statistics are used to identify the $SSED_1$: the greatest depth of erosion for which there is no evidence of a nonzero slope based on the regression. This corresponds to a "breakpoint" in the approach of *Solow* [1987]. When data measured at depths above the $SSED_1$ are included, the slope from the regression is nonzero. We calculate an average steady state erosion rate ($SSER_1$) using the data at $SSED_1$ and below. The choice

Table 2. Summary of Erosion Mill Results[a]

	Total Erosion (mm)		$SSED_1$ (mm)		$SSED_2$ (mm)		$SSER_1$ (g/h)		$SSER_2$ (g/h)	
Sample	Upper	Thalweg	Upper	Thalweg	Upper	Thalweg	Upper	Thalweg	Upper	Thalweg
Sandstone 1	5.35	3.44	3.40	1.76	2.72	1.27	1.99	1.66	1.93	1.68
Sandstone 2	2.63	1.45	1.62	--	1.42	0.38	0.78	0.71	0.73	0.56
Sandstone 3	2.51	1.02	0.84	--	0.90	0.12	0.92	0.37	0.89	0.35
Basalt 1	1.85	0.33	1.39	0.20	1.39	0.17	0.18	0.08	0.17	0.08
Basalt 2	3.03	0.70	1.27	--	0.69	0.08	0.57	0.22	0.53	0.20
Basalt 3	1.56	0.44	0.49	0.24	0.53	0.10	0.43	0.10	0.39	0.09

[a]Subscript 1 indicates results from method 1. Subscript 2 indicates results from Method 2. "--" indicates that method 1 found the SSED to be at the surface: evidence for a non zero slope was not found using any subsets of data.

of including seven data points in the initial test of a slope, as opposed to six for example, is ad hoc. However, with fewer than seven data pairs, the possibility of identifying a slope simply due to a single outlier becomes more likely.

In Figure 3, we show an example of this analysis for Sandstone Upper 2. $SSED_1$ is 1.62 mm, corresponding to 34 h of mill time or the fifteenth mill run. When data from mill runs 15–28 are used in the regression, there is no evidence of a trend in the data. A significant trend does exist ($\alpha < 0.05$) if the abrasion rate from the previous (fourteenth) mill run is included in the regression (runs 14–28). This does not mean that a trend exists in all larger subsets of data, for example, a significant trend does not exist for the subsets that include the twelfth and thirteenth runs (but does for all larger subsets of data).

For two of the sandstone thalweg samples and one of the basalt thalweg samples, significant trends were not observed using any of the subsets of data, including the data from all mill runs in the sequence (Table 2). Therefore, $SSED_1$ is zero, and all the data are used to calculate $SSER_1$. For Sandstone Thalweg 2, this result is clearly inconsistent with a simple qualitative examination of the erosion rate time series (Figure 2). Erosion rates are higher at the beginning of the mill sequence than at the end. A linear trend is not observed when all the data are included in the regression simply because erosion rates from several runs near the beginning of the sequence were relatively low. Clearly, method 1 is not perfect for representing all aspects of the data, which is why we developed method 2 (described below).

We do not attempt to characterize variations in erosion rate above $SSED_1$, beyond simply determining if the initial rate and the average rate above the SSED are higher or lower than the $SSER_1$.

2.3.2. Method 2

The second method provides a different estimate of the steady state erosion depth ($SSED_2$): it is the depth at which erosion rates are first similar to the rates measured at the end of the mill sequence. This approach is based on the observation that erosion rates are relatively steady at the end of the mill sequence (Figure 2). This was shown by method 1: there is no evidence for a linear trend using data from the last seven mill runs for any of the samples.

We complete the following steps for each sample. First, we calculate the mean and standard deviation of the erosion rate over the last seven runs in the sample's mill sequence. The mean is $SSER_2$. Differences exist between $SSER_2$ and $SSER_1$ (Table 2), because the latter is based on all runs beneath the $SSED_1$, which includes more than just the final seven mill runs for all samples. Second, we calculate a threshold to define when the measured erosion rate is approximately equal to $SSER_2$. The threshold is equal to the mean plus the standard deviation over the last seven mill runs (the solid horizontal line in Figure 3, bottom). Third, we move forward through the mill sequence, starting at the beginning, and compare the erosion rate to the threshold. We do not compare rates from a single mill run to the threshold because the data exhibit noise superimposed on the observed trends (Figure 2), likely due to a combination of variations in rock properties, experimental error, and other factors. If we did, a single anomalously low value could fall below the threshold. Instead, we use the mean of three mill runs centered on the depth that is being evaluated. $SSED_2$ is defined as the first depth in the sequence for which the three-sample average is below the threshold.

Figure 3 (bottom) shows how method 2 works for the data from Sandstone Upper 2. The horizontal line shows the threshold for this sample, equal to 0.93 g/h. Moving forward through the sequence, the first mill run for which the centered-average rate (descending black line) is below the threshold is run 12,

corresponding to an $SSED_2$ of 1.42 mm. For this sample, the first single mill run in which the measured rate is below the threshold is also run 12. This is not the case for other samples, when rates from anomalously low individual runs cross the threshold before the centered average. The centered-average rate rises above the threshold again for mill run 15, due to the relatively high value measured during this mill run. The corresponding depth is not used for $SSED_2$ because the threshold was crossed earlier in the sequence.

Method 2 requires a series of ad hoc choices: (1) the number of samples to include in the calculation of the background erosion rate ($SSER_2$), (2) the threshold for defining when $SSED_2$ is crossed, and (3) the averaging window used for comparison to the threshold. We tried various values for all three and found that $SSED_2$ and $SSER_2$ are largely insensitive to these choices. As more samples are included to calculate the erosion rate at the end of the mill sequence, the background erosion rate tends to increase. As a result, the threshold is crossed sooner in the sequence so $SSED_2$ is less.

Methods 1 and 2 yield similar results for the SSED for nearly all samples (Table 2). For the example shown in Figure 3, SSED from the two methods differs by 0.2 mm, or ~10% of the total erosion depth. The most notable difference between the outcomes from the two methods is for the three samples for which method 1 found the SSED to be at the rock surface: samples for which a trend is not found using any of the data. In these cases, $SSED_2$ is small but nonzero, which is more consistent with the pattern shown in the data (discussed below).

We do not estimate the uncertainty in SSED calculated using either method 1 or method 2. Although it would be possible to calculate error estimates, for example, via Monte Carlo sampling across the parameter space, the additional complexity is not warranted given that both methods provide only an approximation of the depth at which erosion becomes steady. Instead, we rely upon the difference in SSED between method 1 and method 2 as a metric of uncertainty. In all cases, the difference in SSED between the two methods is small compared to the differences in SSED between thalweg and upper samples, as shown below.

3. Results

3.1. Qualitative Analysis of Mill Erosion

The total mass removed throughout the sequence of mill runs varied from 15 g for the slowest eroding basalt to $>$200 g for the fastest eroding sandstone. Averaged by rock type, the rate of mass removal from sandstone was approximately 3 times higher than for basalt. The total mass eroded corresponds to an average erosion depth of 0.3 to $>$ 5 mm (Table 2).

Figure 2 displays all of the data from the mill runs. Three patterns are clear. First, for each paired mill run, the erosion rate from the upper sample is almost always higher than from the thalweg sample. These differences are greatest at the beginning of the mill sequence, and then generally decrease in magnitude as erosion proceeds. The differences are much larger than the uncertainty associated with the mill procedure, as shown by the error bars in Figure 2. Second, in all six upper samples, the erosion rate decreases dramatically throughout the experimental cycle. For example, the erosion rate from Sandstone Upper 1 decreases from 5 g/h to 1.5 g/h over 90 h in the mill. The erosion rate from the Basalt Upper 1 decreases by a factor of 50, from $>$ 5 g/h to ~0.1 g/h within the first 76 h of the sequence. In all six upper cases, the changes in erosion rate associated with this general trend are much greater in magnitude than both the random fluctuations between successive measurements and the precision associated with the mill procedure (~0.1 g/h). Third, the erosion rate from all six thalweg samples is relatively constant throughout the experimental cycle, when compared to the changes observed for the upper samples.

Several exceptions are worth noting. For three of the thalweg samples (Sandstone 2, Basalt 1, and Basalt 3), the erosion rate during the first mill run is clearly higher than measured at any other time in the experimental sequence. Some trends throughout the mill sequence also exist. For example, the erosion rate from Sandstone Thalweg 1 tends to increase over the experimental cycle whereas the erosion rates from Basalt Thalweg 1 and 3 appear to decrease through time. These trends are of a much smaller magnitude than those observed for the upper samples.

We now compare mill erosion from each upper-thalweg pair, both averaged throughout the experiment (Figure 4 and Table 2) and averaged through time (Figure 5). For the three sandstone pairs, the mass removed and total erosion depth from the upper samples was 1.6 to 2.5 times greater than for the corresponding thalweg samples (Table 2 and Figure 4, top). For the basalt pairs, the total erosion from the upper samples

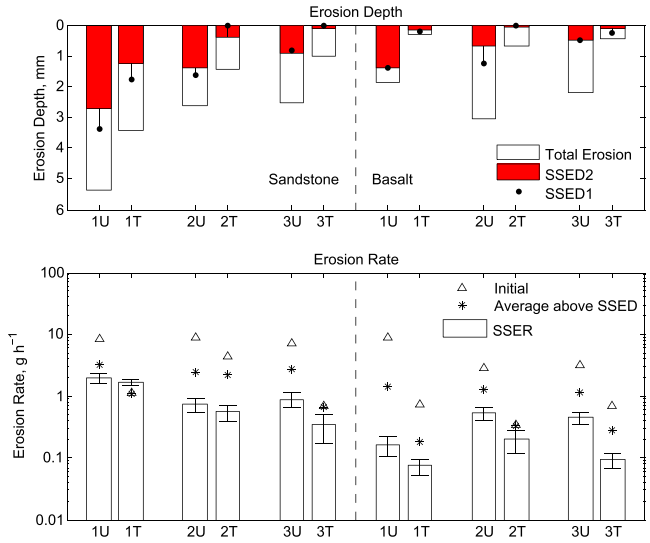

Figure 4. (top) Comparison of total erosion and steady state erosion depth from method 2 (SSED2) for each sample pair. Sample numbers are listed on the *x* axis (U = upper; T = Thalweg). Sandstones are to the left of the vertical dashed line and basalts are to the right. Length of bar (from zero) indicates total erosion. Filled red portion of bar indicates $SSED_2$. The vertical line connects $SSED_2$ to the value from method 1 ($SSED_1$). (bottom) Bar shows $SSER_2$ with ± 1 standard deviation error bars, which is calculated over the last 7 mill runs for each sample. Triangles mark the initial erosion rate (from mill run 1) and asterisks mark the average erosion rate above the $SSED_2$.

was 3.5 to 5.5 times greater than the paired thalweg samples. The ratio of upper-to-thalweg erosion rates generally decreases through time (Figure 5), mostly because erosion rates from upper samples were greatest at the beginning of the mill sequence and subsequently decreased (Figure 2). In Figure 5, we have plotted the ratio of cumulative erosion up to that time in the mill sequence. As a result, these ratios do not converge toward a value of 1 through time, even though the instantaneous erosion rates do tend to converge (Figure 2). The cumulative erosion from the upper samples is 2 to 12 times greater than from the corresponding thalweg samples at the start of the experiment, and largely decreases thereafter. One of the sandstone pairs (Sandstone 2) exhibits a different pattern: the ratio starts around two and increases for the first 12 h before decreasing for the remainder of the mill sequence. The relatively low initial value is due to a high initial erosion rate from the thalweg sample (Figure 2).

3.2. Quantitative Analysis of Mill Erosion

The results described in section 3.1 indicate clear differences between mill erosion from the upper and thalweg samples: erosion rates from upper samples are clearly higher and decrease over the first 50 to 100 h of mill abrasion. We now use the two different methods described in section 2.3 to quantify these variations.

First, we evaluate whether or not the mill erosion rate, and therefore K_r, becomes steady at some measurable depth beneath the rock surface exposed in the stream channel, the SSED. If a SSED exists, we then assess if the erosion rate is greater above this depth, consistent with the expected effects of weathering on K_r. For all six upper samples, a SSED was detected using both methods (Table 2). The SSED for the upper samples varies between 0.5 and 3.5 mm, which is roughly half of the total erosion from each sample (Figure 4). The values found using the two different methods are similar (shown by the bar connecting SSED1 and SSED 2). For all six upper samples, the erosion rate at depths above the SSED is greater than the SSER (Figure 4, bottom). The average erosion rate at depths above the SSED is 2 to 3 times higher than the SSER, except for Basalt 1 where it is nearly 10 times higher. The initial erosion rates are even greater compared to the SSER: the initial erosion rate is ~10 times higher, except for Basalt 1 that is 50 times higher. In summary, for all six upper

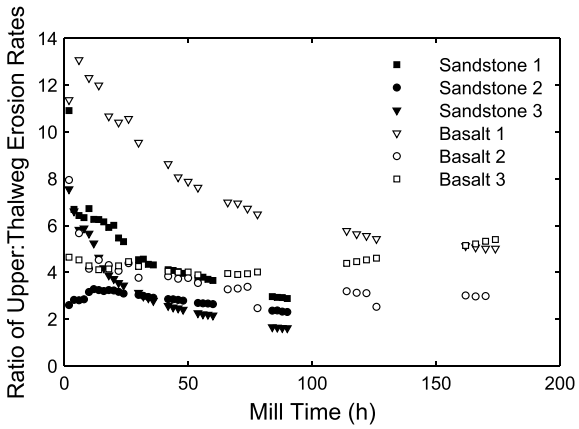

Figure 5. Ratio of upper-to-thalweg cumulative erosion (mass or depth) versus mill time. Cumulative erosion is the total erosion that has occurred up to that time in the mill sequence. Closed symbols are for sandstone pairs, open symbols for basalt pairs.

samples, our analyses clearly show that the erosion rate from the exposed bedrock surface, and presumably rock erodibility (K_r), is greater than that measured 0.5 to 3.5 mm below the rock surface.

The corresponding results from the thalweg samples are similar, although the depth over which erosion rates are enhanced is much less. Based on the first method, three thalweg samples exhibit a SSED and three do not (Table 2). As described in section 2.3, the first method may fail to identify a SSED when there is significant variability relative to the magnitude of the trend (e.g., Sandstone 2, Figure 2). So, the absence of a SSED based on method one alone is questionable. Using method two, a SSED is identified in the erosion data from all six thalweg samples. Method two allows there to be no SSED, specifically when the average erosion rate from the first three runs is within the erosion threshold. Even for sample Basalt 2 (Figure 2), the sample with the initial erosion rate most similar to the remainder of the data in the sequence, the average from the first three runs exceeds the threshold (0.36 g/h versus 0.28 g/h). For five thalweg samples, the SSED is between 0.1 and 0.4 mm. Importantly, the SSED for the thalweg samples is far less than for the corresponding upper samples, and these differences are much larger than the range between SSED calculated using the two different methods (Figure 4). In these five cases, the average erosion rate at depths above $SSED_2$ is 1.5 to 3 times higher than the SSER, whereas the initial erosion rates are 2 to 10 times faster. As with the upper samples, data from the thalweg samples shows that the erosion rate from the exposed bedrock surface is greater than that measured beneath the rock surface. However, the depth over which enhanced erosion is observed is only 0.1–0.4 mm.

The erosion rate data from the Sandstone Thalweg 1 is notably different. The mill erosion rate was ~30% lower at the beginning of the sequence than it was toward the end (Figure 2). A steady state erosion depth was identified via both methods (1.76 and 1.27 mm). The average erosion rate above the SSED and the initial rate are lower than the SSER (Figure 4), which is the opposite of the pattern exhibited by the 11 other samples. However, Figures 2 and 4 show that the differences in erosion rate above and below the SSED are small for Sandstone Thalweg 1, compared to those for all the other samples. A secondary mineral patina, probably calcium sulfate precipitate, encrusted the surface of Sandstone Thalweg 1, likely due to high solute concentrations in the spring-fed baseflow of Onion Creek. This patina was mostly eroded midway through the mill sequence, at the time when the erosion rates stopped increasing and became steady.

Finally, we compare the SSER between each upper-thalweg sample to gauge any similarities or differences between erosion rates once the surface exposed in the streambed is removed. For sandstone pairs 1 and 2, the upper and thalweg SSERs are effectively equal (Table 2 and Figure 4). For sandstone pair 3 and two of the basalt pairs (1 and 2), the upper SSER is roughly twice the thalweg SSER. The upper SSER of the final basalt pair (B3) is approximately 4 times that of the thalweg. In summary, for five of the six sample pairs, the upper SSER is within a factor of 2 of the thalweg SSER. These are small differences compared to either (1) upper-thalweg differences in the initial erosion rate or the average erosion rate above the SSED (Figure 4) or (2) variations in erosion rate for individual samples between the beginning and the end of the mill sequence (Figure 2).

4. Discussion

Data from abrasion mill experiments on bedrock removed from stream channels show two basic results. First, the erosion rate from upper (or channel margin) samples is greater than for thalweg samples. This difference is greatest for the rock surface originally exposed in the stream channel: during the first 2 h mill run, upper samples erode roughly an order of magnitude faster than the corresponding thalweg samples (Figure 4). The contrast in upper-thalweg erosion rates decreases throughout the mill sequence, mostly because erosion rates from the upper samples decrease dramatically throughout the experimental sequence (Figures 2). By the end of the experimental cycle, five of the six sample pairs exhibit erosion rates that are relatively similar (within a factor of approximately 2), while the contrast for the sixth pair is greater. When considered together, these findings show that rock samples from the channel margins are different from those in the thalweg and that these differences are typically greatest at the surface and diminish with depth.

The second result from the abrasion mill experiments is that the erosion rate first decreases with depth and then becomes steady with additional erosion. For the upper samples, there is an order of magnitude decrease in erosion rate over depths of 1–3 mm, below which erosion rate is steady. For thalweg samples, the decrease with depth is limited to the top 0.1–0.4 mm, an amount often removed in the first one or two mill runs. In our

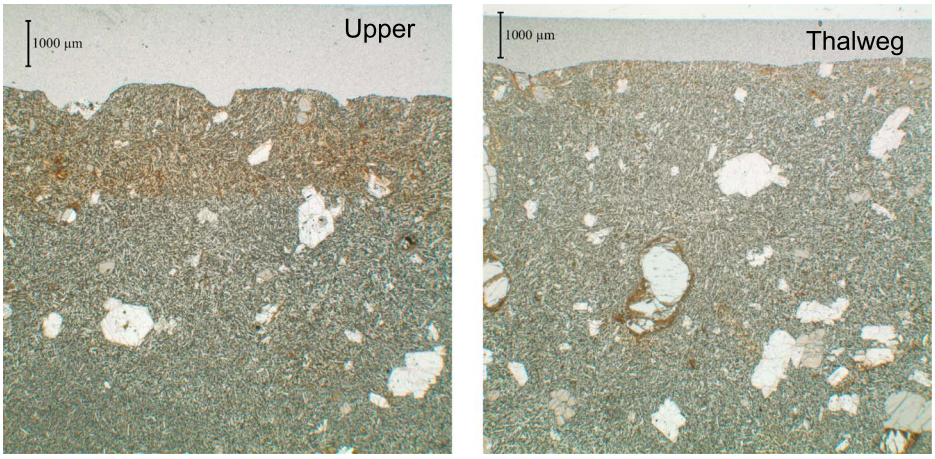

Figure 6. Vertically oriented thin section from (left) Basalt Upper 1 and (right) Basalt Thalweg 1. Photos taken in unpolarized light. The top of the thin section is the channel floor.

experiments, eroded mass was converted to erosion depth based on sample density and the sample area in which the erosion is focused. The latter likely varies between mill runs and samples. In addition, the depth of erosion is not identical throughout the portion of the sample where erosion is focused. Therefore, the reported SSEDs are not absolute measurements of depth. Instead, they should be considered effective depths, representative of an average value for each sample.

As discussed above, the mill erosion rate is considered to be a proxy for K_r: all mill conditions were held constant throughout the experiments except for K_r. The two components of K_r that vary between samples and throughout the mill sequence include the following: (1) the strength of the rock, which controls the erosion rate given some transfer of kinetic energy to the bed [e.g., *Sklar and Dietrich,* 2004] and (2) the surface roughness, which dictates how the saltating bed load interacts with rock surface [e.g., *Huda and Small,* 2014]. In real streams, K_r also includes channel width, which did not vary in the mill.

Based on the abrasion mill results, we propose that K_r varies considerably in each of the channels studied. First, K_r of the bedrock surface exposed in stream channels is higher by an order of magnitude at the channel margins than near the channel center. Second, K_r decreases over depths of several millimeters at the margins of channels, by up to an order of magnitude or more. These variations are large compared to those that could result from variations in climate, and thus weathering, across a drainage basin [e.g., *Han et al.,* 2014]. We expect that these variations in K_r are typical of many bedrock channels. The field sites were selected based on logistical criteria, not because the bedrock in the stream was highly weathered. More extreme cases definitely exist, such as described in *Montgomery* [2004] and *Stock et al.* [2005], where the variations in K_r should be even greater. Measurements of K_r from additional rock types, stream settings, and climates using both the abrasion mill and the alternate methods are needed to more completely assess the variability of K_r.

The simplest explanation for our experimental results is that K_r is enhanced, at the bedrock surface and along the channel margins, due to the effects of weathering on rock strength and/or surface roughness. Several lines of evidence support this idea. First, the observed variations in erosion rate with depth are consistent with the predicted outcome of interactions between weathering and erosion in stream channels [*Howard,* 1998; *Hancock et al.,* 2011]. Second, field observations of rock color, presence of lichen and other biota, and surface roughness at the millimeter scale [*Selby,* 1980] indicate that channel margin bedrock is more weathered than thalweg bedrock. This is more obvious in the photograph from the basalt than from the sandstone channel (Figure 1). Third, for five of the six sample pairs, abrasion rates from the thalweg are similar to those from the channel margin after the surface layer with enhanced erodibility was removed. This indicates that weathering, not upper-to-thalweg differences in lithology, is the likely cause of the high erosion rates measured from the upper samples during the first half of the mill sequence.

For the basalt samples, visual inspection of thin sections provides additional support for the idea that weathering is the source of variations in K_r. Figure 6 shows vertically oriented thin sections from the Basalt 1 sample

pair. For the basalt upper sample, discoloration of the primary mineral grains defines a distinct weathering rind that is approximately 1.5 mm thick. In contrast, for the thalweg sample, discoloration near the surface is less intense, discontinuous, and extends to depths < 0.5 mm. For both samples, localized discoloration around individual mineral grains is observed at greater depths. Importantly, the thickness of the weathering rind is consistent with the SSED determined from the analysis of erosion mill data. X-ray diffraction (XRD) analysis of the upper sample weathering rind indicates a reduction of primary minerals and development of secondary phyllosilicate minerals (Text S2 and Figure S3). In the thalweg sample, XRD analysis of the surface layer reflects the primary mineralogy, indicating only very minor chemical weathering of the exterior.

For the sandstone samples, there is no visible evidence of weathering rind formation or chemical alteration of either the quartz matrix or cement. Of course, the absence of visible alteration in thin sections does not preclude the possibility that chemical weathering processes have lowered the tensile strength of the rock. However, given the composition of the sandstone, it is more likely that weathering increases K_r of the Onion Creek sandstone by increasing the roughness of the bedrock surface. As shown in Figure 1, the roughness associated with bedding planes increases with height above the channel thalweg. We propose that the enhanced mill erosion rates from the sandstone rock surface may be due to the influence of roughness on K_r. As the mill sequence proceeds, roughness is eliminated by mill erosion, and K_r and the mill erosion rates decrease. The observed changes in roughness (~1 mm scale or less) are smaller than the sample-wide changes in surface topography due to the pattern of mill erosion (Figure S1). However, the roughness changes are important because they change the geometry of the grain-bed impacts [e.g., *Huda and Small,* 2014]. In contrast, the topographic variations introduced by the mill are oriented perpendicular to the flow direction, and thus do not directly impact grain impacts and the overall erosion rate.

The abrasion mill experiments described here show clear differences in erosion rate with depth and channel position that are consistent with the expected effects of weathering on rock erodibility. However, several aspects of this study could be improved in future efforts. First, SSED was determined from the time series of "average" erosion depth, calculated from mass removal. The actual erosion depth varied across each sample, so reporting one value of SSED for each sample is a simplification. Second, we did not collect data that is appropriate to quantify the role of evolving surface microtopography on erosion rates throughout the mill sequence (Text S1). Both of these limitations could be addressed with a surface laser scanning system or structure from motion photogrammetry with submillimeter precision, technologies that have become increasingly available since completion of the laboratory experiments described here. Third, the abrasion mill samples are challenging to collect and the mill experiments are labor intensive, so only 12 samples were analyzed from two different bedrock types. Additional samples from more streams are necessary to characterize the spatial variability of rock erodibility in bedrock-floored channels. Alternative methods to estimate rock erodibility should be developed, particularly those that can be applied in the field.

We conclude by discussing the implications of our findings for incision of bedrock-floored channels. The upper-thalweg differences in K_r could reflect greater weathering rates or longer duration of weathering on the channel margins relative to the thalweg. We hypothesize that bedrock above the channel thalweg is more weathered due to the interactions among inundation frequency, variations in erosive power across the channel, and weathering [*Hancock et al.,* 2011]. Typical incision rates in these settings are on the order of ~0.1 mm/yr [*Balco and Stone,* 2005; *Seidl et al.,* 1994], a rate that is consistent with the rate of weathering rind growth [e.g., *Sak et al.,* 2004]. Thus, relatively steady rates of incision in the thalweg will remove weathered material from the bedrock surface as it forms. In contrast, fewer floods inundate bedrock closer to the channel margins, allowing a weathering rind to develop. The extent and depth of weathering will increase at the channel margins until either (1) a particularly large flood occurs or (2) the bedrock surface becomes so erodible that more frequent, smaller floods yield appreciable erosion. The presence of a distinct ~1 mm deep zone of enhanced K_r suggests that weathered material is not completely removed during these events. Instead, a balance develops between weathering-enhanced erodibility and episodic incision to allow channel margins to lower at rates similar to the thalweg [e.g., *Hancock et al.*, 2011]. Variability in rock erodibility across bedrock channel margins, shown here for the first time, may have a significant impact on steady state channel geometry and gradient. We suggest that weathering-induced changes in rock erodibility within bedrock channels adds an additional degree of freedom, like the extent of bedrock exposure within the channel [e.g., *Sklar and Dietrich,* 2001; *Johnson and Whipple,* 2010], in the adjustment of channels to uplift, substrate, and climate.

Our observation that rock erodibility, K_r, may vary spatially across channels has several implications for modeling the evolution of bedrock-floored channels. Model simulations show that the interaction between weathering and erosion within channels determines how erodibility varies across a channel, and this variability determines in part the steady state channel width and channel gradient [*Hancock et al.,* 2011]. However, stream power laws used to simulate bedrock channel evolution are based on the assumption that (1) K_r is spatially and temporally constant for a given lithology and (2) channel width can be modeled as a simple power law function of drainage area [see *Gasparini and Brandon,* 2011]. With these simplifying assumptions, channel adjustments are limited to changes in profile gradient. Similarly, channel and landscape evolution models incorporating process-based channel erosion schemes that are more faithful to the mechanics of rock erosion processes [e.g., *Wobus et al.*, 2006; *Crosby et al.,* 2007; *Turowski et al.,* 2007; *Gasparini et al.,* 2007] assume that erodibility is a constant. As a result, these models neglect the role of changes in erodibility driven by weathering and the changes in channel width that result [*Hancock et al.,* 2011].

5. Conclusions

Laboratory abrasion mill experiments on bedrock surfaces extracted from streams with sandstone and basaltic bedrock demonstrate the following. First, the erosion rate from channel margin samples is greater than for thalweg samples. The greatest difference exists for the rock surface that was exposed in the stream channel. Second, erosion rate decreases with depth beneath the original rock surface, by up to an order of magnitude. The erosion rate becomes steady at depths of 1–3 mm for channel margin samples and 0.1–0.4 mm for thalweg samples. These results suggest that rock erodibility of the bedrock surface exposed in these stream channels is higher at the margins than near the channel center and that erodibility decreases over depths of ~1 mm. The simplest explanation for these patterns is that erodibility is enhanced, at the bedrock surface and along the channel margins, due to the effects of weathering on rock strength and surface roughness. These types of variations in erodibility are not considered in most models of bedrock stream erosion, but could influence how channels respond to tectonic and climatic forcings.

Acknowledgments
This project was supported by NSF Geomorphology and Land Use Dynamics grants EAR 0922235 (E.S. and C.W.) and EAR 0922026 (G.H.). Three anonymous reviewers provided useful comments and suggestions. The data for this paper are available by contacting the corresponding author.

References

Allen, G. H., J. B. Barnes, T. M. Pavelsky, and E. Kirby (2013), Lithologic and tectonic controls on bedrock channel form at the northwest Himalayan front, *J. Geophys. Res. Earth Surf.*, *118*, 1806–1825, doi:10.1002/jgrf.20113.

Aydin, A., and A. Basu (2006), The use of Brazilian test as a quantitative measure of rock weathering, *Rock Mech. Rock Eng.*, *39*(1), 77–85, doi:10.1007/s00603-005-0069-0.

Balco, G., and J. O. H. Stone (2005), Measuring middle Pleistocene erosion rates with cosmic-ray-produced nuclides in buried alluvial sediment, Fisher Valley, southeastern Utah, *Earth Surf. Processes Landforms*, *30*(8), 1051–1067, doi:10.1002/esp.1262.

Craddock, W. H., D. W. Burbank, B. Bookhagen, and E. J. Gabet (2007), Bedrock channel geometry along an orographic rainfall gradient in the upper Marsyandi River valley in central Nepal, *J. Geophys. Res.*, *112*, F03007, doi:10.1029/2006JF000589.

Crosby, B. T., K. X. Whipple, N. M. Gasparini, and C. W. Wobus (2007), Formation of fluvial hanging valleys: Theory and simulation, *J. Geophys. Res.*, *112*, F03S10, doi:10.1029/2006JF000566.

Duvall, A., E. Kirby, and D. Burbank (2004), Tectonic and lithologic controls on bedrock channel profiles and processes in coastal California, *J. Geophys. Res.*, *109*, F03002, doi:10.1029/2003JF000086.

Gasparini, N. M., and M. T. Brandon (2011), A generalized power law approximation for fluvial incision of bedrock channels, *J. Geophys. Res.*, *116*, F02020, doi:10.1029/2009JF001655.

Gasparini, N. M., K. X. Whipple, and R. L. Bras (2007), Predictions of steady state and transient landscape morphology using sediment-flux-dependent river incision models, *J. Geophys. Res.*, *112*, F03S09, doi:10.1029/2006JF000567.

Han, J., N. Gasparini, J. Johnson, and B. Murphy (2014), Modeling the influence of rainfall gradients on discharge, bedrock erodibility, and river profile evolution, with application to the Big Island, Hawai'i, *J. Geophys. Res. Earth Surf.*, *119*, 1418–1440, doi:10.1002/2013JF002961.

Hancock, G., E. Small, and C. Wobus (2011), Modeling the effects of weathering on bedrock-floored channel geometry, *J. Geophys. Res.*, *116*, F03018, doi:10.1029/2010JF001908.

Hancock, G. S., R. S. Anderson, and K. X. Whipple (1998), Beyond power: Bedrock river incision process and form, in *Rivers Over Rock: Fluvial Process in Bedrock Channels*, *Geophys. Monogr. Ser.*, vol. 107, edited by K. J. Tinkler and E. E. Wohl, pp. 35–60, AGU, Washington, D. C.

Hartshorn, K., N. Hovius, W. B. Dade, and R. L. Slingerland (2002), Climate-driven bedrock incision in an active mountain belt, *Science*, *297*(5589), 2036–2038, doi:10.1126/science.1075078.

Heimsath, A. M., W. E. Dietrich, K. Nishiizumi, and R. C. Finkel (1997), The soil production function and landscape equilibrium, *Nature*, *388*(6640), 358–361, doi:10.1038/41056.

Howard, A. D. (1994), A detachment-limited model of drainage-basin evolution, *Water Resour. Res.*, *30*(7), 2261–2285, doi:10.1029/94WR00757.

Howard, A. D. (1998), Long profile development of bedrock channels: Interaction of weathering, mass wasting, bed erosion, and sediment transport, in *Rivers over Rock: Fluvial Process in Bedrock Channels*, *Geophys. Monogr. Ser.*, vol. 107, edited by K. J. Tinkler and E. E. Wohl, pp. 297–319, AGU, Washington, D. C.

Howard, A. D., and G. Kerby (1983), Channel changes in badlands, *Geol. Soc. Am. Bull.*, *94*(6), 739–752, doi:10.1130/0016-7606(1983)94<739:ccib>2.0.co;2.

Huda, S. A., and E. E. Small (2014), Modeling the effects of bed topography on fluvial bedrock erosion by saltating bed load, *J. Geophys. Res. Earth Surf.*, *119*, 1222–1239, doi:10.1002/2013jf002872.
Johnson, J. P. L., and K. X. Whipple (2010), Evaluating the controls of shear stress, sediment supply, alluvial cover, and channel morphology on experimental bedrock incision rate, *J. Geophys. Res.*, *115*, F02018, doi:10.1029/2009JF001335.
Lague, D. (2014), The stream power river incision model: Evidence, theory and beyond, *Earth Surf. Processes Landforms*, *39*(1), 38–61, doi:10.1002/esp.3462.
Matsuoka, N. (1990), The rate of bedrock weathering by frost action—Field-measurements and a predictive model, *Earth Surf. Processes Landforms*, *15*(1), 73–90, doi:10.1002/esp.3290150108.
Montgomery, D. R. (2004), Observations on the role of lithology in strath terrace formation and bedrock channel width, *Am. J. Sci.*, *304*(5), 454–476, doi:10.2475/ajs.304.5.454.
Phillips, J. D., A. V. Turkington, and D. A. Marion (2008), Weathering and vegetation effects in early stages of soil formation, *Catena*, *72*(1), 21–28, doi:10.1016/j.catena.2007.03.020.
Sak, P. B., D. M. Fisher, T. W. Gardner, K. Murphy, and S. L. Brantley (2004), Rates of weathering rind formation on Costa Rican basalt, *Geochim. Cosmochim. Acta*, *68*(7), 1453–1472, doi:10.1016/j.gca.2003.09.007.
Scheingross, J. S., F. Brun, D. Y. Lo, K. Omerdin, and M. P. Lamb (2014), Experimental evidence for fluvial bedrock incision by suspended and bedload sediment, *Geology*, *42*(6), 523–526, doi:10.1130/g35432.1.
Seidl, M. A., W. E. Dietrich, and J. W. Kirchner (1994), Longitudinal profile development into bedrock—An analysis of Hawaiian channels, *J. Geol.*, *102*(4), 457–474.
Selby, M. J. (1980), Rock mass strength classification for geomorphic purposes: With tests from Antarctica and New Zealand, *Z. Geomorphol.*, *24*, 31–51.
Sklar, L. S., and W. E. Dietrich (2001), Sediment and rock strength controls on river incision into bedrock, *Geology*, *29*(12), 1087–1090, doi:10.1130/0091-7613(2001)029<1087:sarsco>2.0.co;2.
Sklar, L. S., and W. E. Dietrich (2004), A mechanistic model for river incision into bedrock by saltating bed load, *Water Resour. Res.*, *40*, W06301, doi:10.1029/2003WR002496.
Solow, A. R. (1987), Testing for climate change—An application of the 2-phase regression-model, *J. Climate Appl. Meteorol.*, *26*(10), 1401–1405, doi:10.1175/1520-0450(1987)026<1401:tfccaa>2.0.co;2.
Stock, J. D., D. R. Montgomery, B. D. Collins, W. E. Dietrich, and L. Sklar (2005), Field measurements of incision rates following bedrock exposure: Implications for process controls on the long profiles of valleys cut by rivers and debris flows, *Geol. Soc. Am. Bull.*, *117*(1–2), 174–194, doi:10.1130/b25560.1.
Tucker, G. E. (2004), Drainage basin sensitivity to tectonic and climatic forcing: Implications of a stochastic model for the role of entrainment and erosion thresholds, *Earth Surf. Processes Landforms*, *29*(2), 185–205, doi:10.1002/esp.1020.
Turowski, J. M., D. Lague, and N. Hovius (2007), Cover effect in bedrock abrasion: A new derivation and its implications for the modeling of bedrock channel morphology, *J. Geophys. Res.*, *112*, F04006, doi:10.1029/2006JF000697.
Turowski, J. M., N. Hovius, M.-L. Hsieh, D. Lague, and M.-C. Chen (2008a), Distribution of erosion across bedrock channels, *Earth Surf. Processes Landforms*, *33*(3), 353–363, doi:10.1002/esp.1559.
Turowski, J. M., N. Hovius, A. Wilson, and M.-J. Horng (2008b), Hydraulic geometry, river sediment and the definition of bedrock channels, *Geomorphology*, *99*(1–4), 26–38, doi:10.1016/j.geomorph.2007.10.001.
Turowski, J. M., D. Lague, and N. Hovius (2009), Response of bedrock channel width to tectonic forcing: Insights from a numerical model, theoretical considerations, and comparison with field data, *J. Geophys. Res.*, *114*, F03016, doi:10.1029/2008JF001133.
Whipple, K. (2004), Bedrock rivers and the geomorphology of active orogens, *Annu. Rev. Earth Planet. Sci.*, *32*, 151–185, doi:10.1146/annurev.earth.32.101802.120356.
Whipple, K. X., N. P. Snyder, and K. Dollenmayer (2000a), Rates and processes of bedrock incision by the Upper Ukak River since the 1912 Novarupta ash flow in the Valley of Ten Thousand Smokes, Alaska, *Geology*, *28*(9), 835–838, doi:10.1130/0091-7613(2000)28<835:rapobi>2.0.co;2.
Whipple, K. X., G. S. Hancock, and R. S. Anderson (2000b), River incision into bedrock: Mechanics and relative efficacy of plucking, abrasion, and cavitation, *Geol. Soc. Am. Bull.*, *112*(3), 490–503, doi:10.1130/0016-7606(2000)112<0490:riibma>2.3.co;2.
Wobus, C. W., G. E. Tucker, and R. S. Anderson (2006), Self-formed bedrock channels, *Geophys. Res. Lett.*, *33*, L18408, doi:10.1029/2006GL027182.
Wohl, E. E., K. R. Vincent, and D. J. Merritts (1993), Pool and riffle characteristics in relation to channel gradient, *Geomorphology*, *6*(2), 99–110, doi:10.1016/0169-555x(93)90041-y.